Astronomy
&
Astrophysics

Numerical methods for non-LTE line radiative transfer:
Performance and convergence characteristics

G.-J. van Zadelhoff[1], C. P. Dullemond[2], F. F. S. van der Tak[3], J. A. Yates[4], S. D. Doty[5], V. Ossenkopf[6],
M. R. Hogerheijde[7], M. Juvela[8], H. Wiesemeyer[9], and F. L. Schöier[1]

[1] Leiden Observatory, PO Box 9513, 2300 RA Leiden, The Netherlands
[2] Max Planck Institut für Astrophysik, Postfach 1317, 85741 Garching, Germany
[3] Max Planck Institut für Radioastronomie, Auf dem Hügel 69, 53121 Bonn, Germany
[4] University College London, Gower Street, London WC1E 6BT, UK
[5] Department of Physics and Astronomy, Denison University, Granville, OH 43023, USA
[6] 1. Physikalisches Institut, Universität zu Köln, Zülpicher Str. 77, 50937, Köln, Germany
[7] Steward Observatory, The University of Arizona, 933 N. Cherry Ave. Tucson AZ 85721, USA
[8] Helsinki University Observatory, Tähtitorninmäki, PO Box 14, 00014 University of Helsinki, Finland
[9] Institut de Radio-Astronomie Millimétrique, 300 rue de la piscine, Domaine Universitaire, 38406 St. Martin d'Hères, France

Abstract. Comparison is made between a number of independent computer programs for radiative transfer in molecular rotational lines. The test models are spherically symmetric circumstellar envelopes with a given density and temperature profile. The first two test models have a simple power law density distribution, constant temperature and a fictive 2-level molecule, while the other two test models consist of an inside-out collapsing envelope observed in rotational transitions of HCO^+. For the 2-level molecule test problems all codes agree well to within 0.2%, comparable to the accuracy of the individual codes, for low optical depth and up to 2% for high optical depths ($\tau = 4800$). The problem of the collapsing cloud in HCO^+ has a larger spread in results, ranging up to 12% for the $J = 4$ population. The spread is largest at the radius where the transition from collisional to radiative excitation occurs. The resulting line profiles for the HCO^+ $J = 4$–3 transition agree to within 10%, i.e., within the calibration accuracy of most current telescopes. The comparison project and the results described in this paper provide a benchmark for future code development, and give an indication of the typical accuracy of present day calculations of molecular line transfer.

Key words. stars: formation – molecular processes

1. Introduction

Molecular lines are excellent probes of the physical and chemical conditions in interstellar clouds, protostellar envelopes, circumstellar shells around late-type stars, photon-dominated regions etc. Furthermore, molecular line transitions play a key role in probing the properties of galaxies and their evolution. The interpretation of such lines requires the use of line radiative transfer programs which can calculate accurately the non-LTE (local thermodynamic equilibrium) level populations and the resulting output spectra. See Black (2000) for a recent review.

It is known from stellar atmosphere research that subtle errors in radiative transfer algorithms can lead to significantly incorrect results (Mihalas 1978). A particularly well-known problem of this kind is an insufficiently stringent convergence criterion at high optical depths. In the absence of a posteriori checks on numerical results, the best way to validate the

methods is by the use of various techniques, if possible with many independent codes of different types. Once the reliability and the behavior of the codes has been established and understood, they can be safely used within the limits of parameter space within which tests have been carried out.

In this paper, the setup and results of a large-scale campaign to compare line radiative transfer programs are described. The test problems are spherically symmetric, and can be modeled by a 1-dimensional radiative transfer code. Codes capable of handling more than one dimension could be compared in a similar way in the future.

The main aim of this paper is to examine and compare the various radiative transfer methods that are currently used in the astrophysical community for modeling the shape and strength of molecular lines emerging from interstellar and circumstellar matter. A series of problems is chosen that represent the difficulties that may be encountered in comparison with data from present-day and future ground-based telescopes, such as the Sub-Millimeter Array (SMA), the Atacama Large Millimeter

Array (ALMA) and future airborne and space-borne missions such as SOFIA and the Herschel Space Observatory. The test problems and their solutions presented here are available to the community via a web-site, allowing users to run the same problems, check the accuracy of their codes and thus speed up the further development of their own radiative transfer codes. It is hoped that this will stimulate a more widespread use of these codes for the interpretation of molecular line observations.

We present two test problems, each at two different optical depths (i.e. in total four problems). The first problem is a fictive 2-level molecule in a spherical envelope with a powerlaw density with no systematic velocity and a constant temperature. This problem is meant to tune all codes before examining the more complex, realistic problem. The main test problem is based on the 1-dimensional (1-D) inside-out collapse model, where the level populations are computed for HCO^+ at various abundances. The HCO^+ ion is chosen as a representative example of the molecule which samples gas with a large range in densities and is readily observable in a variety of astrophysical regions. Both a high and a low optical depth model, representative of the main isotope HCO^+ and the less abundant isotope $H^{13}CO^+$, are used to check the convergence properties of each code. All test problems and their results can be found at the webpage `http://www.strw.leidenuniv.nl/~radtrans`.

2. Molecular line radiative transfer

The radiative transfer problem is represented by an equation describing the emission, absorption and movement of photons along a straight line in a medium:

$$\frac{dI_\nu}{ds} = j_\nu - \alpha_\nu I_\nu \tag{1}$$

with the notation adopted from Rybicki & Lightman (1979). Equation (1) is the differential description of the intensity I_ν along a photon path (ds) at frequency ν, where j_ν [erg s^{-1} cm^{-3}] and α_ν [cm^{-1}] denote the emission and absorption coefficients. Another way of writing Eq. (1) is:

$$\frac{dI_\nu}{d\tau_\nu} = S_\nu - I_\nu, \tag{2}$$

where $S_\nu = j_\nu/\alpha_\nu$ is referred to as the source function (the emissivity of the medium per unit optical depth), and the optical depth τ_ν is defined in differential form as $d\tau_\nu = \alpha_\nu ds$. Equation (2) can be written in integral form, which is the form that is most often used in radiative transfer codes:

$$I_\nu(\tau) = \int_0^\tau S_\nu(\tau') e^{\tau'-\tau} d\tau', \tag{3}$$

where τ is the optical depth between the point where I_ν is evaluated and spatial infinity along the line (i.e., $s = -\infty$). This integral is evaluated along all possible straight lines through the medium. In practice, these will be a discrete sample of lines covering space and direction as well as possible.

For the problem of molecular line transfer the emission and absorption coefficients are determined by the transition rates between the various rotational and/or vibrational levels of the molecule, and the population of these levels. For a transition from level i to level j (where the energy of level i is greater than that of level j) the emission and absorption coefficients are given by:

$$j_{ij}(\nu) = n_i A_{ij} \phi_{ij}(\nu), \tag{4}$$

$$\alpha_{ij}(\nu) = (n_j B_{ji} - n_i B_{ij})\phi_{ij}(\nu), \tag{5}$$

where n_i and n_j [cm^{-3}] are the population densities of the upper (i) and lower (j) level, and A_{ij}, B_{ij} and B_{ji} are the Einstein coefficients. The function $\phi_{ij}(\nu)$ represents the line profile for this transition, which is properly described as a Voigt profile, a combination of a (micro-turbulent) Gaussian and intrinsic Lorentzian line broadening.

The source function for a particular transition S_{ij} is independent of velocity if one assumes complete frequency redistribution, i.e., the frequency deviation from line center of absorbed and emitted photons are uncorrelated. The source function then becomes:

$$S_{ij} = \frac{j_{ij}(\nu)}{\alpha_{ij}(\nu)} = \frac{n_i A_{ij}}{n_j B_{ji} - n_i B_{ij}}. \tag{6}$$

The relative level populations n_i are determined from the statistical equilibrium equation:

$$\sum_{j>l}\left[n_j A_{jl} + (n_j B_{jl} - n_l B_{lj})\overline{J}_{jl}\right] - \sum_{j<l}\left[n_l A_{lj} + (n_l B_{lj} - n_j B_{jl})\overline{J}_{lj}\right]$$

$$+ \sum_j \left[n_j C_{jl} - n_l C_{lj}\right] = 0, \tag{7}$$

where $C_{ij} = n_{col}K_{ij}$ with K_{ij} the collisional rate coefficients in cm^3 s^{-1} and n_{col} the density of collision partners, taken here to be H_2 in $J = 0$. $\overline{J}_{jl}$ is the integrated mean intensity over the line profile:

$$\overline{J}_{ij} = \frac{1}{4\pi} \int I_\nu(\Omega) \phi(\nu) d\Omega \, d\nu. \tag{8}$$

The symbol Ω represents the spatial direction in which the intensity $I_\nu(\Omega)$ is measured.

A useful concept for the analysis of radiative transfer calculations is the excitation temperature T_{ex} of the transition between level i and level j, given by

$$T_{ex} = \frac{-h\nu_{ij}}{k}\left[\ln\left(\frac{g_j}{g_i}\frac{n_i}{n_j}\right)\right]^{-1}, \tag{9}$$

where k is Boltzmann's constant and g_i the statistical weight of level i. The energy difference between the two levels is given by $h\nu_{ij}$. In local thermodynamic equilibrium (LTE), T_{ex} equals the local gas temperature, while if T_{ex} higher or lower, the excitation is super- or sub-thermal. In addition, the intensity is proportional to T_{ex} in the optically thin limit.

Equations (3)–(8) form a coupled set of equations. The way in which the quantities depend on each other is depicted in Fig. 1. The intensities are found by integrating the source function (Eq. (3)). The source function and extinction coefficients depend on the level populations (Eqs. (4)–(5)). These in turn depend on the intensities (Eqs. (7)–(8)). To solve this set of equations one must determine the radiation field and the level populations simultaneously. Since the radiation field couples
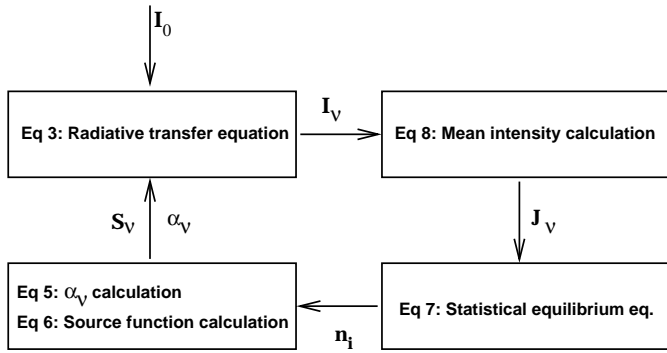
Fig. 1. Flow diagram of the molecular line radiative transfer problem. Since the problem is coupled (follow arrows), several iterations are needed to calculate the true level populations n_i. All adopted symbols are explained in Sect. 2

the level populations at different spatial positions to each other through the transfer integral (Eq. (3)), the only way of solving this system directly seems to be through complete linearization and solving a huge matrix equation involving all level populations at all spatial positions. In practice, the evaluation of the matrix elements and the inversion of the problem consumes far too much CPU-time as well as memory and is therefore beyond current computing capabilities. An alternative and much simpler way is to iteratively evaluate all equations, following the arrows, as illustrated in Fig. 1. This method is called "Lambda Iteration" and includes formal integral codes as well as Monte Carlo methods. Though simple, its principal disadvantage is that it converges slowly at high optical depths. Many radiative transfer codes therefore use a hybrid scheme: the direct inversion of a simplified subset of the equations, and iteration to solve the remaining problem. In this paper we have used codes of the Lambda Iteration type (including Monte Carlo methods), of the "Complete Linearization" type, and hybrid schemes such as "Approximate/Accelerated Lambda Iteration" and "Accelerated Monte Carlo".

3. Methods and codes

In this paper four methods and eight different codes are compared. Any practical method discretizes the problem to determine the level populations at each position. A short description is given in this section of each of these codes. The first method (LI) is not used, but given as an introduction for the other methods. In Table 1, the different codes and principal authors are indicated. Detailed descriptions of each of the codes can be found in the references given.

3.1. Lambda Iteration (LI)

The Lambda Iteration method is the most basic method of all. It involves the iterative evaluation of level populations and intensities until the system has converged. The name "Lambda Iteration" originates from the fact that the process of iteration can be mathematically written into a formalism involving a "Lambda Operator". This Lambda Operator represents the

entire procedure of computing the line-weighted mean intensities $\overline{J}_{ij}$ from the source function. It involves the formal integral Eq. (3) along all possible lines through the medium, and includes the angle-frequency integrations of Eq. (8) to obtain the $\overline{J}$. The Lambda Operator is defined as:

$$\overline{J}_{ij} = \Lambda_{ij}[S_{ij}], \qquad (10)$$

and is therefore a global operator. The Λ_ν operator is a matrix operator connecting all points and all levels to each other. To solve the radiative transfer numerically, the problem has to be discretized both in space and frequency and initial level populations have to be assumed. With these level populations, the Lambda Operator is constructed by solving the radiative transfer for I_ν and $\overline{J}$, which is inserted in Eq. (7) to calculate the new level populations. The procedure is repeated until the relative change in the level populations or mean intensities between two successive steps falls below a desired convergence criterium. The time to reach convergence of the solution is proportional to τ^2 for $\tau \gg 1$ and is therefore extremely slow for highly optically thick regions. The very small local changes in the level populations in successive iterations could then be easily mistaken for convergence.

3.2. Monte Carlo (MC)

The Monte Carlo (MC) method is based on the simulation of basic physical processes with the aid of random numbers. This makes the formalisms of these codes relatively simple and intuitive as one has to deal only with the basic formulae. But one must take proper care of the statistics and be sure that all regions in space and frequency are well sampled by the randomly distributed photon packages. The Monte Carlo method for molecular line transfer has been described by Bernes (1979) for a spherically symmetric cloud with a uniform density. A major advantage of MC codes is the possibility of non-regular grids, in particular for multi-dimensional problems. In fact, MC methods are straightforward to extend from 1-D to 2-D (Hogerheijde & van der Tak 2000) and even 3-D (Park & Hong 1998; Juvela 1997). One of the major disadvantages of the method is the long CPU time which is needed to lower the random error intrinsic in the method. This error decreases inversely proportional to the square root of the number of simulated photons. In addition, the method suffers from similar convergence problems as Lambda Iteration, as it is formally a variant of the Lambda Iteration method.

Thus far, the Monte Carlo method has been implemented in two ways. In one set of codes, the radiation field is randomly sampled by discrete photons that are emitted and absorbed in the material. In the other set, the radiation field is sampled by random directions along which the radiative transfer is evaluated.

3.3. Approximated/Accelerated Lambda Iteration (ALI)

This scheme is similar to the Lambda iteration scheme, with the difference that the equations are pre-conditioned to speed up the convergence. The simplest (but still highly efficient) way to

implement the ALI scheme is by splitting the Lambda Operator into the local self-coupling contribution and the remainder:

$$\Lambda_{ij} = (\Lambda_{ij} - \Lambda_{ij}^*) + \Lambda_{ij}^* \qquad (11)$$

with Λ_{ij} the lambda operator between the i and j levels and Λ_{ij}^* the diagonal (local), or tridiagonal (local+nearest-neighbor), part of the full Lambda operator. In general more reliable convergence properties are obtained with tridiagonal or higher bandwidths (Hauschildt et al. 1994). Since an approximate operator Λ_{ij}^* of this kind is easily invertible, and since its matrix elements are relatively easy to calculate, one can use this operator for the matrix inversion, and use the iteration for solving the remainder (non-local part) of the transfer problem. Since the self-coupling of a cell at high optical depth is the bottleneck that slows down convergence in Lambda Iteration codes, this removal of the local self-coupling by direct inversion of Λ_{ij}^* can speed up the convergence drastically. A full description of the method was given by, e.g., Rybicki & Hummer (1991, 1992).

In addition to this operator splitting technique, one can apply certain iteration-improvement schemes such as the Ng-acceleration method (Ng 1974). These are methods that can improve the convergence of any linearly converging iteration scheme. In the Ng-method one uses the previous results to estimate the convergence behavior of the problem. After every four iteration steps an extrapolation can then be performed towards the expected convergence. The number of iterations is not a strict requirement but four is typically found to give a reliable and significant acceleration. This scheme is very effective as can be seen in Figs. 1 to 3 in Rybicki & Hummer (1991), where the number of iterations is plotted versus the convergence.

3.4. Accelerated Monte Carlo (AMC)

The difference in Accelerated Monte Carlo and Monte Carlo methods can be similarly described as the ALI compared to LI method. Most important is the splitting of the mean intensity in an external field and a local contribution. Formally,

$$\overline{J} = (\Lambda - \Lambda^*)[S_{ul}^{\dagger}(\overline{J})] + \Lambda^*[S_{ul}(\overline{J})] \qquad (12)$$

$$= \overline{J}^{\text{external}} + \overline{J}^{\text{local}} \qquad (13)$$

$$= \frac{1}{N}\sum_i I_{0,i}e^{-\tau_i} + \frac{1}{N}\sum_i S_{ul}[1 - e^{-\tau}] \qquad (14)$$

with $S_{ul}^{\dagger}(\overline{J})$ the results from the previous iteration and N the number of photons. This is an important issue as in the standard Monte Carlo approach, most time is taken by photons trapped in an optically thick cell, where due to absorption and randomly directed emission the photons follow a random walk path through the cell, with one step for each iteration.

The splitting can be done in different ways. Juvela (1997) implements a diagonal lambda operator in Eqs. (12)–(14) by counting explicitly those photons which were emitted and absorbed within the same cell. A reference field described by Bernes et al. (1979) is used to decrease the random fluctuations caused by the Monte Carlo sampling. Hogerheijde & van der Tak (2000) perform sub-iterations to

calculate the local contribution in each cell, thus ensuring that in each cell the local field and populations are always consistent with the external field due to all other cells. A third possibility of acceleration, adopted by Schöier (2000), is the use of core-saturation (Rybicki 1972; Hartstein & Liseau 1998), where optically thick line center photons are replaced by the local source function.

3.5. Local linearization (MULTI type codes)

This method was developed by Scharmer & Carlsson (1985) and Harper (1994) to produce the MULTI and SMULTI line radiation transport codes respectively. This approach perturbs Eqs. (2) to (8) linearly, neglecting second order or higher terms. The linearization greatly reduces the effect of high optical depth terms and allows rapid convergence. The MULTI and SMULTI codes use the Olson diagonal approximate operator (Olson et al. 1986) scheme to save on storage. This operator uses the diagonal of the Λ matrix when computing the solution to the linearized equations. Although this adds in approximations and delays convergence, it greatly reduces the required storage capacity and so for many problems it allows the problem to be tackled in the first place. Olson's scheme simply assumes that the changes in the intensity are related to the changes in the source and opacity terms (the level populations). The main difference to the other schemes is that the solution to the linearized equations returns changes, δn and δJ to the level populations and the mean intensities respectively. There is always the possibility that a converged solution contains unphysical negative populations, and this provides a useful indicator for poor sampling and errors. In the version used here a ALI-type scheme to complement the MULTI is used, providing numerical stability but also slower convergence in optically thick media.

3.6. Radiative transfer codes

Each code described in this paper uses one or more of the above techniques to calculate a converged set of level populations. In this section we list the codes which use each of the convergence methods listed above. Then for each code we describe how convergence is accelerated, how each code samples the volume under consideration, and state the convergence criteria used by each code.

1. Monte Carlo (MC):
   - F. Schöier (Schöier 2000); the rate of convergence depends on the number of model photons and the iterative procedure. In the problems presented here, the counters of stimulated emission are reset after each set of 5 iterations. The number of iterations needed for convergence in the "classical" Monte Carlo scheme is of the same order as the maximum optical depth in the model. The core saturation method is included to speed up the convergence in the high optical depth case. To reach an accuracy of $\sim 10^{-2}$ in the derived level populations, $\sim 10^5 - 10^6$ model photons per iteration are generally needed in the optically thick case.

Table 1. Codes used.

Label[1]	Author	method	dimensions	Reference
A	Juvela	AMC	1D, 2D & 3D	Juvela (1997)
B	Hogerheijde & van der Tak	AMC	1D & 2D	Hogerheijde & van der Tak (2000)
C	Schöier	MC	1D	Schöier (2000)
D	Doty	ALI	1D	
E	Ossenkopf	ALI	1D & 2D	Ossenkopf et al. (2001)
F	Dullemond	ALI	1D & 2D	Dullemond & Turolla (2000)
G	Yates	(S)MULTI	1D	Rawlings & Yates (2001)
H	Wiesemeyer	ALI	1D & 2D	Wiesemeyer (1997)

[1] Label used in Figs. 4 and 6 for each of the codes.

2. Accelerated Lambda Iteration (ALI):

– V. Ossenkopf (Ossenkopf et al. 2001); all discretizations are done by the code such that sufficiently small differences between the grid points are guaranteed. This concerns the radial shells, the grid of rays, the frequency grid, and the number of levels used. The convergence is measured in terms of radiative energy densities, not level populations, which are extrapolated from the Auer acceleration scheme. Locally, the code may take into account turbulent sub-clumping using the statistical description of Martin et al. (1984), but this is not used here.

– S. Doty; the input data are interpolated onto the spatial grid of the problem with a variable method (log/linear/combined). This, coupled with extreme care in the ray-tracing integration, helps to ensure high accuracy. A local approximate lambda operator and Ng acceleration are used to solve both the line and continuum transfer. Convergence is determined by changes in both level populations and the local net heating rate, with small ($\leq 10^{-4}$) changes required for the entire spatial grid for both accelerated and non-accelerated iterations.

– C.P. Dullemond (Dullemond & Turolla 2000); the formal integration proceeds via a short-characteristics method using the three-point quadrature formula of Olson & Kunasz (1987). The discrete local angles μ_i are chosen using the tangent-ray prescription. This means that successive short characteristics match up and no interpolations are required. At every grid point there are 41 angular points in μ with three extra around $\mu \simeq 0$ to prevent undersampling. Using the ALI method with a local operator and Ng acceleration, the system is iterated towards a solution with a convergence criterion 10^{-6} in level population.

– H. Wiesemeyer (Wiesemeyer 1997); the rate of convergence is improved by applying the method of minimization of residuals (Auer 1987). Other acceleration methods, such as vector and matrix extrapolation, are currently being implemented. The solution to the equation of radiative transfer is evaluated by various numerical methods (either quadrature rules, or multi-value methods), according to the accuracy required by the problem to be solved. The code uses long characteristics, to preserve an isotropic distribution of rays at any point of the model volume, following the multivariate quadrature rule of Steinacker et al. (1996). Its performance is thus rather optimized to solve smooth problems in more than one dimension. All discretizations are performed by the code.

3. Accelerated Monte Carlo (AMC):

– M. Juvela (Juvela 1997); this code uses the reference field method to reduce random fluctuations. The velocity is discretized into 50 channels and the number of rays per iteration was taken to be 350. The ray generation is weighted such that the same number of rays was shot through each annulus. The random number generators are reset after each iteration, making it possible to use Ng acceleration on every third iteration starting with the fifth iteration. Convergence was tested only for the eight lowest levels down to 1×10^{-3} in level population.

– M. Hogerheijde & F. van der Tak (Hogerheijde & van der Tak 2000); in this code, one cell at a time is considered, with N rays entering the cell from random directions. The radiative transfer is followed along each of these rays, starting with the CMB field at the edge of the cloud. In this way it is possible to calculate separately the local contribution to the radiation field in the target cell, allowing significant reduction of the computing time for optically thick cells. For a first order estimate of the radiation field, the same set of random numbers is used to describe the ray directions for each iteration, thus resembling a fixed-ray (ALI) code. This process yields a solution free of random noise but with possible inadequate sampling of directions and velocities. In the second stage a different set of random numbers is used for each iteration, providing true random sampling of the radiation field. The number of rays is increased for each cell until convergence is reached, ensuring proper angular sampling of the radiation field everywhere. The equations of statistical equilibrium are solved in each iteration to a fractional error of 10^{-6} in all levels except the highest. The user specifies a signal-to-noise ratio S; the MC noise is reduced by increasing the number of photons such that the fractional error of

the levels between iterations is smaller than $1/S$. For the test problem, $S = 100$ was used.

4. Complete linearization (MULTI-type):

 – J. Yates (Rawlings & Yates 2001); in the problems presented, the SMMOL code used 400 rays through the cloud to compute the intensities at each radial grid-point in the spherical cloud using a finite difference method to compute the intensities. The grid sampling along each ray can adapt simply to take account of large changes that affect the optical depth, typically caused by velocity changes along the ray. In this calculation, typically 100 grid-points were used to sample the full absorption profile. The SMMOL codes uses a convergence criterion of 1×10^{-4} for both the level populations and the mean intensities.

4. Description of the test models

4.1. Models 1a/1b: A simple 2-level molecule

The first two test problems (problems 1a/1b) have a simple and cleanly defined setup without velocity gradients and using a constant temperature and line width. Complicating factors such as a different treatment of the spatial grid and frequency sampling are thus kept to a minimum, so that every code should in principle be able to solve these problems down to their specified accuracy.

The simple 2-level molecule test setup consists of a spherically symmetric cloud with a power law hydrogen number density specified by

$$n_{\mathrm{H_2}}(r) = n_{\mathrm{H_2}}(r_0) \left(\frac{r}{r_0}\right)^{\alpha} \quad \mathrm{cm}^{-3}, \tag{15}$$

where r is the radius in cm. We take $n_{\mathrm{H_2}}(r_0) = 2.0 \times 10^7 \mathrm{cm}^{-3}$, $r_0 = 1.0 \times 10^{15}$ cm and $\alpha = -2$. The kinetic temperature of this problem is taken to be constant: $T_{\mathrm{kin}}(r) = 20$ K. The abundance of the molecule (which we will specify below) is constant as well: $X_{\mathrm{mol}}(r) \equiv n_{\mathrm{mol}}(r)/n_{\mathrm{H_2}}(r) = X_{\mathrm{mol}}$, and the systematic velocity is zero everywhere. The spherically symmetric cloud ranges from $r_{\mathrm{in}} = 1.0 \times 10^{15}$ cm to $r_{\mathrm{out}} = 7.8 \times 10^{18}$ cm. For $r < r_{\mathrm{in}}$ and for $r > r_{\mathrm{out}}$ the density is assumed to be zero. The incoming radiation at the outer boundary is the $T = 2.728$ K microwave background radiation.

We choose a fictive 2-level molecule which is specified by

$$E_2 - E_1 = 6.0 \mathrm{cm}^{-1} = 8.63244 \mathrm{K} \tag{16}$$

$$g_2/g_1 = 3.0 \tag{17}$$

$$A_{21} = 1.0 \times 10^{-4} \mathrm{s}^{-1} \tag{18}$$

$$K_{21} = 2.0 \times 10^{-10} \mathrm{cm}^3 \mathrm{s}^{-1} \tag{19}$$

in which the downward collision rate is $C_{21} = n_{\mathrm{H_2}} K_{21} \mathrm{s}^{-1}$. The total (thermal+turbulent) line width a is given by $a = 0.150 \mathrm{km s}^{-1}$. The line profile is assumed to be a Gaussian:

$$\phi(\nu) = \frac{c}{a\nu_0 \sqrt{\pi}} \exp\left(-\frac{c^2(\nu - \nu_0)^2}{a^2 \nu_0^2}\right) \tag{20}$$

where c is the speed of light in units of km s^{-1}, and ν_0 is the frequency at line center.

We solve the problem for two different abundances:

Problem 1a: $\quad X_{\mathrm{mol}} = 1.0 \times 10^{-8}$

Problem 1b: $\quad X_{\mathrm{mol}} = 1.0 \times 10^{-6}$.

Problem 1a is a simple case with a moderate optical depth ($\tau \simeq 60$ from star to infinity at line center). Problem 1b has much higher optical depth ($\tau \simeq 4800$) and is therefore numerically stiffer.

This problem was originally described and worked out by Dullemond & Ossenkopf (see Dullemond 1999).

4.2. Models 2a/2b: A collapsing cloud in HCO⁺

The second two problems (problems 2a/2b) are examples of problems typically encountered in the field of sub-millimeter molecular line modeling. These problems have much of the complicated physics included, such as velocity- and temperature gradients, non-constant line widths, multiple levels etc. Moreover, the problem is based on a numerical model provided externally, and therefore introduces the complication of a given intermediate-resolution spatial grid. The resulting spread of the results therefore gives a good indication of how accurate the predicted line strengths and shapes for a typical every-day-life model calculation are.

The model on which these "realistic" test problems are based was constructed by Rawlings et al. (1992, 1999) to analyze HCO⁺ data for an infalling envelope around a protostar. The prototypical example of such a "class 0" young stellar object is B335. The model describes how the cloud core collapses from the inside-out. Starting from a nearly isothermal sphere in pressure balance, a perturbation triggers the center of the cloud to collapse. This sends out a rarefaction wave at the local speed of sound, which causes the outer parts of the cloud to collapse as well. The model is similar to the analytical inside-out collapse model by Shu (1977), but includes more realistic physics. No rotation is assumed, which makes it ideal for a 1-D spherical comparison.

Figure 2 shows the structure of the cloud at a particular time during the collapse phase. This is the input model for our test cases. The collapse can clearly be seen in the radial velocity, which is 0 for radii greater than 10^{17} cm, and directed towards the source for smaller radii. The density profile is given by a power-law of the form $n(r) = n_0(r/r_0)^m$, where $m = -1.5$ inside the collapsing sphere ($r < 10^{17}$ cm) and $m = -2.0$ outside. The model parameters are specified at 50 radii logarithmically spaced between 10^{16} and 4.6×10^{17} cm.

The infall of a cloud has a significant influence on the molecular line emission. The lines will be skewed to the blue, or double peaked with a stronger blue-shifted component, depending on the velocity field and optical depth of the line (e.g. Myers et al. 2000). This feature can be intuitively understood because the foreground gas has a lower excitation temperature than the background gas. This only holds when the foreground gas is optically thick enough in the line. Otherwise a single-peaked lineshape, centered on the source velocity, results.

For the comparison presented here, the ion HCO⁺ is used, where an abundance compared to H_2 is adopted of 1×10^{-9} for
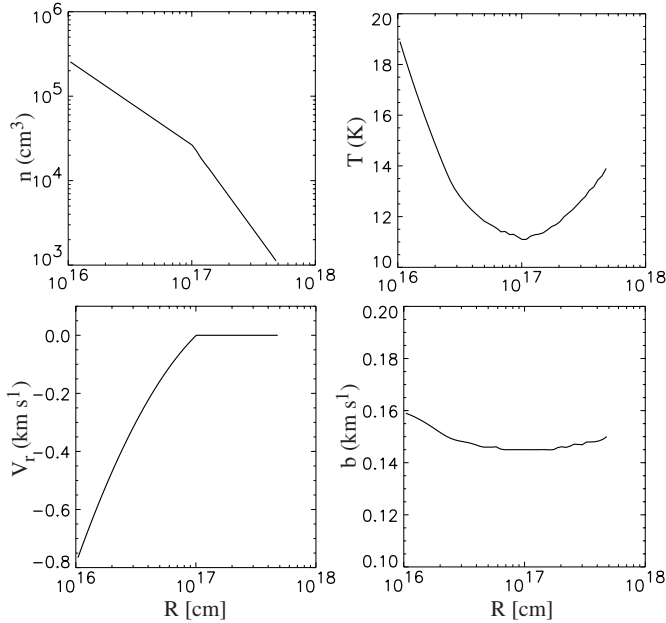
Fig. 2. Physical structure of the test model 2. Upper left: density, lower left: velocity, upper right: temperature, lower right: turbulent line width b [km s^{-1}]. Changes in the density and velocity distributions are seen at the point where infall starts. The temperature of the gas at the inside rises due to the infall while the outside is heated by the interstellar radiation.

problem 2a, and 1×10^{-8} for problem 2b. This causes the optical depths τ for the lowest 4 transitions to range from 0.1 to 10 for problem 2a, and from 1 to 100 for problem 2b. A common file of Einstein-A coefficients and collisional rate coefficients of HCO$^+$ with H$_2$ in $J = 0$ (Monteiro 1985; Green 1975) has been used in all models. These can be downloaded from `http://www.strw.leidenuniv.nl/~radtrans`. 21 levels of the HCO$^+$ ion are included in the model. Since the rate coefficients are temperature dependent, all downward (upper→lower) rate coefficients are given for a number of temperatures (10, 20, 30, 40 K). At each temperature, a linear interpolation is performed to calculate the local downward collisional rate coefficients. Performing this interpolation accurately is extremely important because the exponential relation between the excitation and de-excitation coefficients can introduce large deviations. The upward (lower→upper) collisional rate coefficient is subsequently calculated using the detailed balance relation,

$$\frac{C_{lu}}{C_{ul}} = \frac{g_l}{g_u} e^{E_{ul}/kT}. \tag{21}$$

The fact that the molecular data, in particular the collisional rate coefficients, are not known with infinite precision introduces an additional uncertainty in the solution of the radiative transfer equations. The use of different collisional rate coefficients has an impact on the level populations and thereby on the strength of the predicted emission lines. However, the spread in available rate coefficients in the literature has no effect on the comparison presented here, as all the codes use the same molecular data as input. On a webpage `http://www.strw.leidenuniv.nl/~moldata`

molecular files for a large number of molecular species will be made available in the future (Schöier et al., in preparation), including a comparison of different rates from the literature and their effect on the model results.

With these sets of problems the different codes are tested on the following features:

- Convergence of the code;
- Radiative transfer in optically thin lines;
- Radiative transfer in optically thick lines;
- Sampling of the radiation transfer in the presence of a velocity field;
- Incorporation of the cosmic microwave background radiation ($T_{CMB} = 2.728$ K), which influences the lower levels near the outside of the cloud.
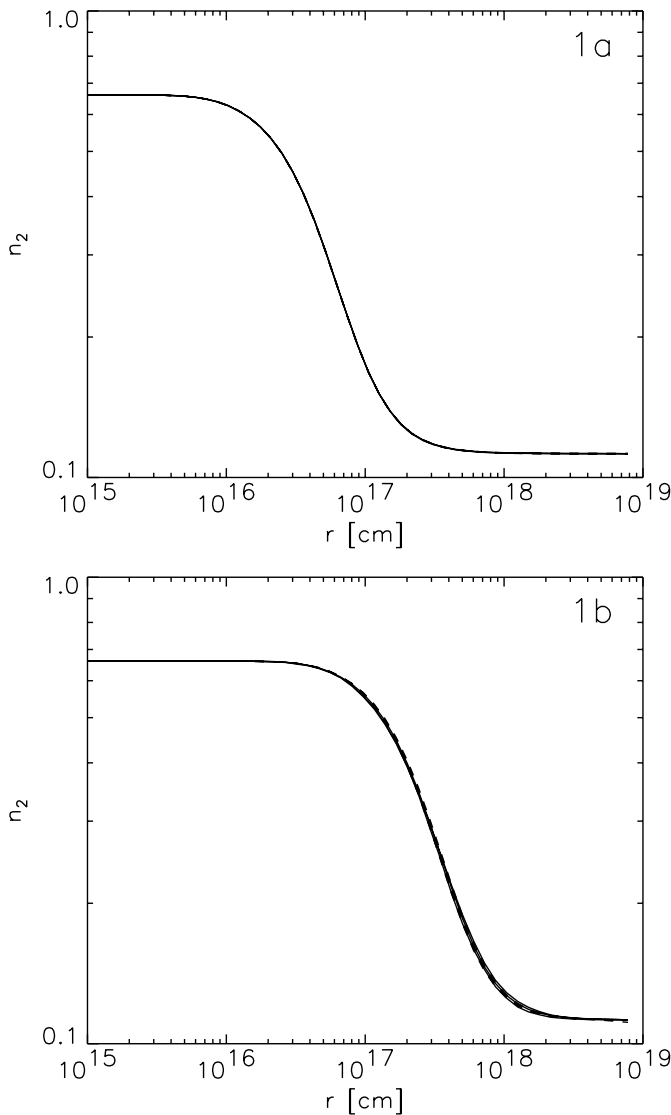
5. Results

5.1. Results of problems 1a/1b

Test problems 1a and 1b are relatively simple in the sense that no velocity gradients and temperature variations are present. Also, since the problem setup is specified analytically, the grid resolution can be chosen to be as high as required for the particular code the participant is using. By virtue of the zero systematic velocity, the treatment of the inner boundary is not much of an issue, because the line is perfectly thermalized at that radius. These test problems therefore purely test the radiative transfer as such.

The results for the problems 1a and 1b are shown in Fig. 3. The interior of the cloud is completely thermalized ($T_{ex} = T_{kin}$). The decline of n_2 at larger radii is due to the departure from LTE. At the outer radii the population again saturates to a constant value, which is due to the microwave background radiation ($T_{ex} = T_{CMB}$). All codes agree reasonably well, although small differences remain distinguishable. The relative differences between the codes are shown in Fig. 4 in comparison to the mean.

If we consider the "mean" solution to be the correct one, then the typical errors are of the order of a few percent or less. The errors are clearly greater for problem 1b than for problem 1a. This is to be expected, since problem 1b has higher optical depth and is therefore numerically more challenging. For problem 1a, the codes show a small spread with a standard deviation of 0.2%. i.e. they agree with each other to within 2×10^{-3} relative difference, comparable to the accuracy criteria of the codes, clearly visible in the noise for the Monte Carlo results. For problem 1b the best agreement reached between the codes shows a standard deviation with a local maximum of 2% ($\Delta n_2/n_2 \sim 2 \times 10^{-2}$). To achieve maximum accuracy, the codes used a spatial resolution of $(R_{i+1} - R_i)/R_i \simeq 0.05$ for this problem, but this high spatial resolution did not reduce the spread between the codes to the 10^{-3} level.

For problem 1b (the most difficult of the two) an ALI code with Ng acceleration with spatial resolution $(R_{i+1} - R_i)/R_i \simeq 0.04$ typically takes about 160 iterations to meet the converge criterion of $\Delta n_2/n_2 < 10^{-7}$. The same problem, but for a less stringent convergence criterion ($\Delta n_2/n_2 < 10^{-4}$) and for a lower spatial resolution ($(R_{i+1} - R_i)/R_i \simeq 0.2$) typically takes

Fig. 3. Results of the two-level molecule problems. Shown here are the populations of the upper level of the 2-level molecule. Top panel: problem 1a. Bottom panel: problem 1b. Plotted are the (A)MC codes, denoted by solid lines and the ALI/SMULTI codes using dashed lines.

about 40 iterations. The relative error introduced by the lower spatial resolution and lower convergence criterion for this problem is at most 1%, provided that second-order (or higher) integration of the transfer equation is used. The use of first-order integration introduces errors of the order of 12%, even for the high-resolution runs. For test problem 1a, at low resolution and with a weak convergence criterion ($\Delta n_2/n_2 < 10^{-4}$), an ALI code typically uses 18 iterations.

For the AMC-type codes with Ng acceleration (Juvela 1997), problem 1b typically requires about 75 iterations, with about 120 photon packages (rays) per iteration. It was found that the application of Ng acceleration at the very start of the iteration had a negative influence on the convergence rate. Good convergence was achieved by applying Ng only after about 25 iterations. As in the case of the ALI type codes, problem 1a was much more benign: 15 iterations with about 120 photon packages (rays) per iteration.

It should be said that the AMC-type codes allow considerable freedom in how to disentangle the number of iterations and the number of photon packages per cell per iteration. Therefore the numbers given here may vary from code to code, i.e., in most codes the number of photon packages per iteration per cell is used. For the accelerated Monte Carlo codes, acceleration of the convergence only operates when some of the cells are optically thick. If all cells are optically thin but the entire source optically thick, the local radiation field becomes negligible compared to the overall radiation field and separating local and global contributions no longer effectively speeds up convergences.

The SMULTI code converged to below 10^{-4} in 30 iterations and to below 10^{-5} in 50 iterations for the second model. For the first model the code converged in 10 iterations.

5.2. Results of problems 2a/2b

5.2.1. Level populations

The results for the test problems 2a and 2b are shown in Fig. 5. The direct comparison is shown for two different levels of HCO$^+$, $J = 1$ and $J = 4$. These levels were chosen because they represent the emitting levels of two easily and often observed lines of the molecule probing different density regimes. The $J = 1-0$ line lies at millimeter wavelengths at 89 GHz and the critical density of the $J = 1$ level is 3.4×10^4 cm^{-3}. The $J = 4-3$ line occurs in the sub-millimeter at 356 GHz, with a critical density for exciting the $J = 4$ level of 1.8×10^6 cm^{-3}. The different model results are plotted on top of each other, together with one additional calculation where the CMB radiation field was deliberately ignored. In the level populations, the effect of the CMB is visible as a lack of excitation of the $J = 1$ level in the outer regions. The figure immediately shows that in the outer region, the excitation at line center of the $J = 1-0$ line is controlled by the CMB field and not by the local temperature and density. The $J = 1$ level lies only 4.3 K above ground, close to the T_{CMB} (2.728 K) temperature, so that the 1–0 transition can be effectively excited by the peak of the CMB radiation. The density in the outer regions of the collapsing cloud is too low for the molecule to be excited to LTE. The $J = 4$ level population is less affected by the CMB radiation field.

To show a more quantitative measure of the accuracy of the results, the level populations are plotted versus their difference to the mean of all the results (Fig. 6). Only results including the CMB radiation field are used to calculate the mean. At the inner boundary, the solutions diverge into two main groups. This is a result from the inner boundary condition adopted by the different authors. The density and temperature of the test problem were not specified within the inner radius and were either chosen as an empty sphere or a non-rotating sphere of constant density. The different solutions near the inner boundary have a relatively small error (Fig. 6) showing that in this case the inner boundary has little influence on the overall solution and can be ignored in the specification of the problem.

The calculated populations of the $J = 1$ level show a standard deviation ranging from 2% close to the star down to 1.5% for problem 2b and below 1% in problem 2a. The $J = 4$ level
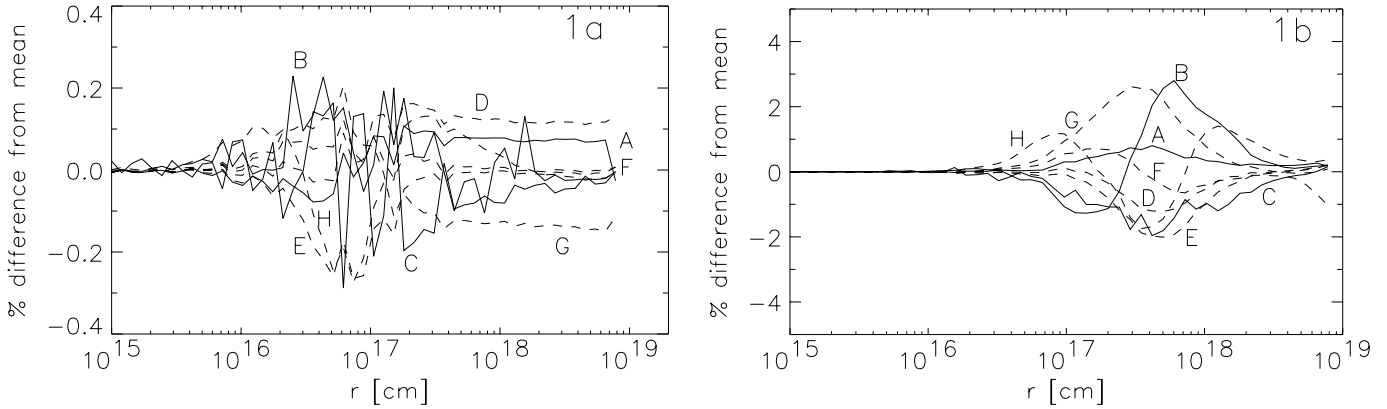
Fig. 4. As Fig. 3, but now shown as the relative difference from the average of the results for problems 1a (left) and 1b (right). Plotted are the (A)MC codes, denoted by solid lines and the ALI/SMULTI codes using dashed lines. The notation for each of the codes is given in Table 1. Note that the differences between the codes is of the same order as the Monte Carlo noise for problem 1a, indicating that the codes have converged to the correct level.
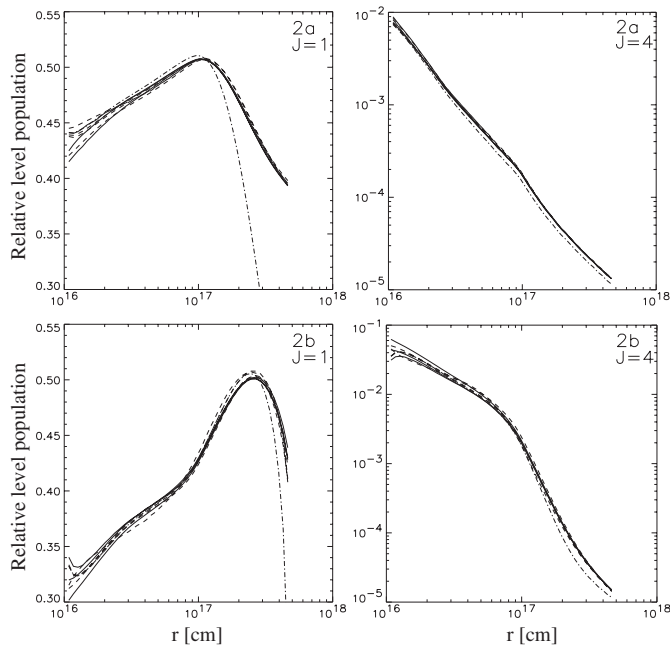
Fig. 5. Populations of levels $J = 1$ and $J = 4$ in the optically thin (model 2a) and optically thick (model 2b) cases. The dotted line is the solution where no cosmic background radiation was added, the solid lines represent the (A)MC-based codes and the dashed lines the ALI-based codes. Due to the low temperatures and densities of the problem, most molecules are in the lowest rotational states. Only codes A–G participated in this comparison.

has a larger spread with a standard deviation of 8% close to the inner boundary up to 12% at $r = 2 \times 10^{17}$ cm and down to 2% at the outer boundary for the high τ (problem 2b) case. The HCO$^+$ lines have high critical densities and the $J = 4$ level population is far from LTE. In addition, the optical depth is high, making the calculation for the 4–3 line particularly difficult. In problem 2a the $J = 4$ level rises from 3% close to the inner boundary up to 4% in the transition region and down to 1% close to the outer boundary. Lacking an analytical solution, we take the average of the numerical results as the best estimate of the

exact solution. The deviations from the average therefore give an estimate of the implicit and explicit approximations of the codes. Fitting models to observational data with criteria better than these deviations will not lead to more accurate estimates of the physical parameters.

For all the problems, the level populations were also calculated using LI by Dullemond and Wiesemeyer. The populations agreed within the errors as shown in Figs. 4 and 6 for the low τ cases. However in both the 1b and 2b problems the solution was not reached using similar convergence criteria as the ALI calculations. Even though the LI method itself should in principle find the same solution, the number of iterations and more strict convergence criteria make it a numerically too costly task to solve.

The problem is particularly sensitive to the gridding of the physical parameters. A comparison of two runs, where one had twice as many gridcells, showed a significant decrease of the error compared to the mean value for one of the Monte Carlo code (C). This shows the importance of a correct gridding of the problem.

5.2.2. Excitation temperature

As a second comparison, the excitation temperature (Fig. 7) is plotted for all solutions, which may be a more intuitive manner to show the results. When level populations are in LTE, the excitation temperature equals the local kinetic temperature. Comparing the results with Fig. 2b, the excitation temperature of the 1–0 line is close to LTE near the inner boundary but becomes subthermal at larger radii. The $J = 4–3$ excitation temperature is always well below its LTE value, which is due to its much higher critical density. As Fig. 7 shows, the excitation temperature never drops below 2.728 K, except in the case where the CMB radiation was ignored. In the inner region ($r < 5 \times 10^{16}$ cm), the excitation of the $J = 1$ level is dominated by collisions, while in the outer parts, it is dominated by radiation. The transition region between these two extremes shows the largest differences in the results (Fig. 6a).
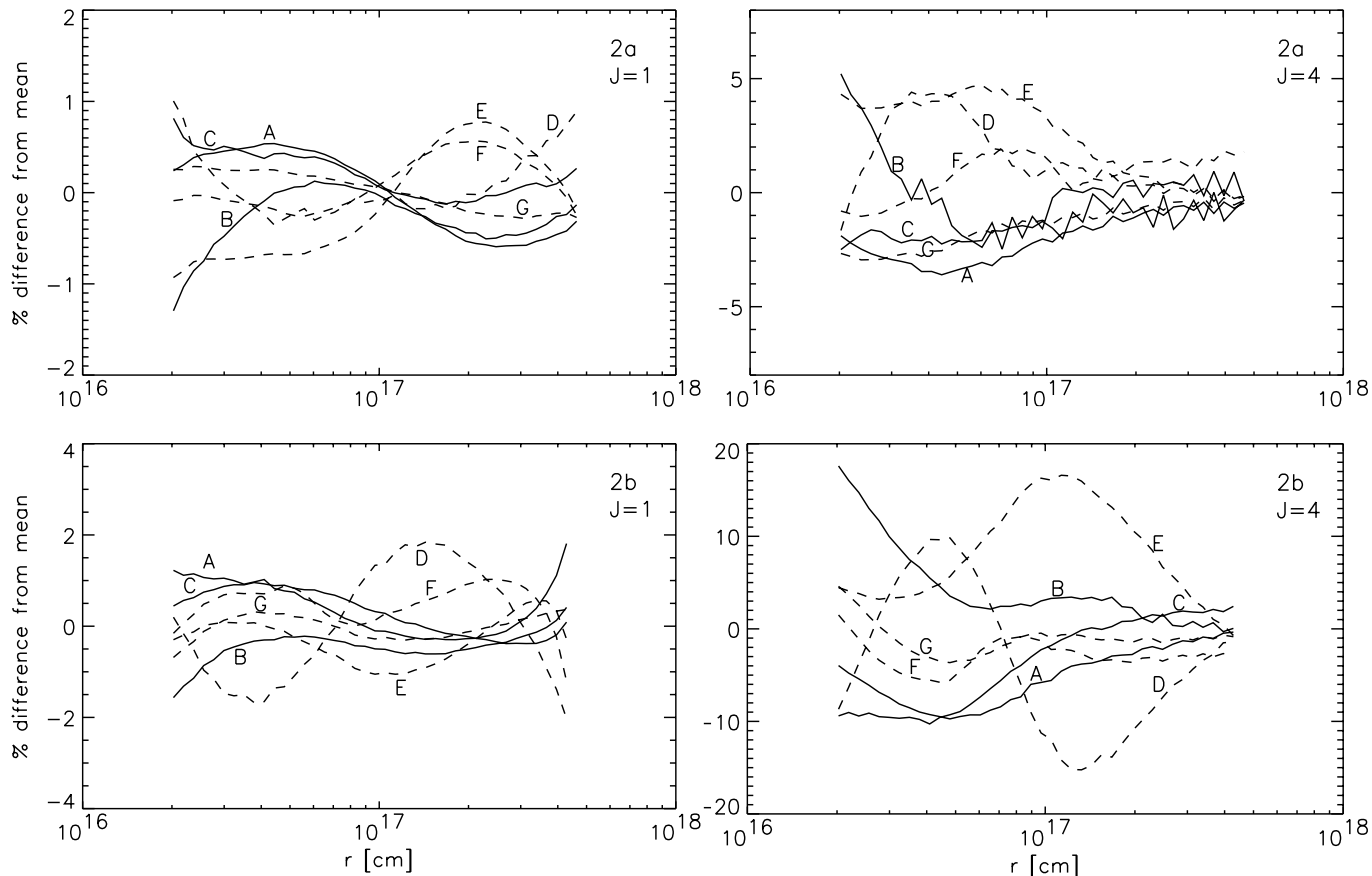
Fig. 6. Differences of the populations in the $J = 1$ and $J = 4$ levels to the mean for both model 2a and 2b. The solid lines represents the (A)MC based codes and the dashed lines the ALI based codes. The notation of each of the lines is given in Table 1. Only codes A–G participated in this comparison.

5.2.3. Line profiles

Figure 8 compares the results in terms of the line profiles. The calculated level populations at each position in the cloud are used to compute the velocity profiles of the selected lines using a program which calculates the sky brightness distribution. To ensure an equivalent emitting mass, the inner sphere is assumed to be empty for all models. The profiles are calculated by constructing a plane through the origin of the cloud perpendicular to the line of sight, with a spatial resolution small enough to sample the physical distributions. A ray-tracing calculation is performed through this plane from $-\infty$ to $+\infty$, keeping track of the intensity in the different velocity bins. For this calculation the program SKY was used, part of the RATRAN code (http://talisker.as.arizona.edu/~michiel/). By applying a single common code for these calculations, no secondary uncertainties are introduced. The resulting sky brightness distribution is convolved with a beam of 14″ for the $J = 4$–3 transition, appropriate for the James Clerk Maxwell Telescope (JCMT) at this frequency. For the $J = 1$–0 transition, the beam size is taken to be 29″ representative of the IRAM 30 m telescope. The distance is assumed to be 250 pc.

Comparison of Figs. 8a and 8c shows that increasing the abundance of HCO$^+$ by a factor of 10 changes the $J = 1$–0 peak intensity by only a factor of 2.5. The $J = 1$–0 line

becomes more self-absorbed, indicating that the line has indeed become more optically thick. The $J = 4$–3 emission line is optically thin for the low abundance, as seen from its single-peaked profile in Fig. 8b. The more optically thick model shows the characteristic asymmetric line structure, skewed to the blue. The differences in the level populations are visible in the line profiles. In the $J = 1$–0 line profiles (Fig. 8c) all solutions lie on top of each other in the line wings and only a slight difference can be seen at line center. The error is largest in the region with low velocities represented by the larger errors in the center of the line profile. The integrated intensity profiles differ by a few % for low τ and 6–7% for the high τ case. The error is in general larger for the $J = 4$ level, which shows up as a larger error in the integrated lines for the $J = 4$–3 transition. For low τ the error is $\approx 2\%$, but for high optical depths deviations up to 12% are found for the most outlying case. Although substantial, these differences are generally less than the current calibration uncertainties of the observational data, which are typically 20% to 30%.

The differences in the profiles shown here give a rough indication of the quality of fitting necessary to interpret observational data. It should be noted that some differences are likely due to different implementations of the cloud model. One can fit a model precisely to an observational data set using a particular radiative transfer code; however the results will not
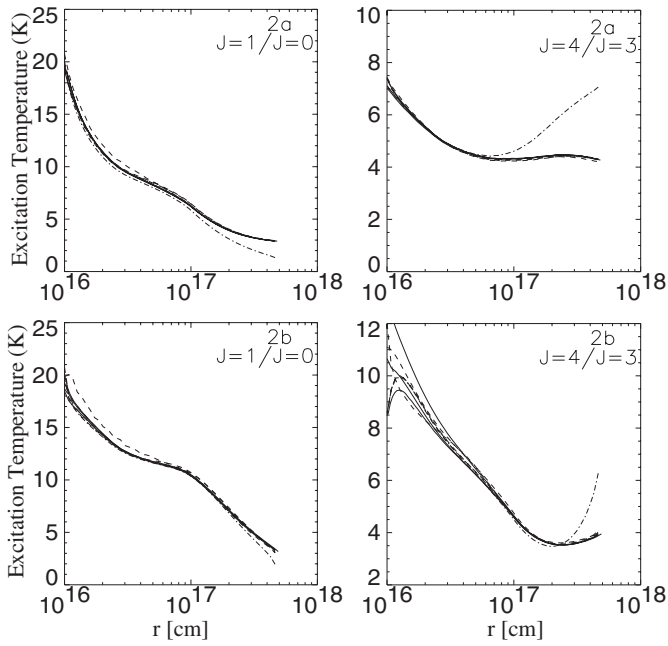
Fig. 7. Excitation temperatures [K], as defined in Eq. (9), for the levels $J = 1/J = 0$ and $J = 4/J = 3$. Top panels: low optical depth case (problem 2a); bottom panels: high optical depth case (problem 2b). The dotted line indicates the model result with the CMB radiation neglected, the solid lines represent the (A)MC-based codes and the dashed lines the ALI-based codes. When the lines are in LTE, the excitation temperature is equal to the kinetic temperature (Fig. 2).
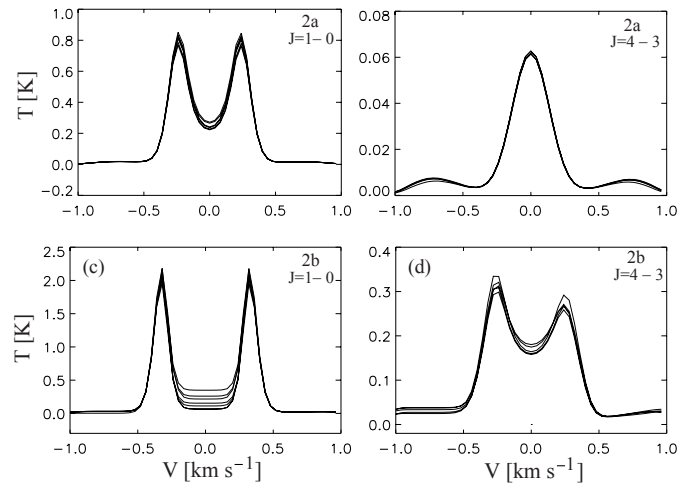

Fig. 8. Calculated intensity [K] of the $J = 1-0$ and $J = 4-3$ lines for the problems 2a and 2b. In the high optical depth case (lower two panels), the blue-shift or "infall asymmetry" is visible. The low resolution of the spatial grid becomes apparent in the line emission at ± 0.75 km s^{-1}.

necessarily be the same if a different code is used. The derivation of physical parameters is therefore always limited in accuracy to the error bars given by the code itself in comparison to other codes.

6. Discussion and conclusion

In spite of the fact that the spread in our solutions lies within the accuracy limits of current-day (sub-)millimeter instruments, it is important to understand how this spread comes about. The first two test cases were defined analytically, and avoided difficulties of gridding as much as possible. The small spread of these results, even at high optical depths, seems to show that in principle the radiative transfer is done correctly by all codes. The larger spread in the HCO$^+$ collapsing cloud problem can therefore be attributed to the problem of gridding, both in space and in frequency. The coarse spatial gridding in the setup of the problem, and the presence of strong velocity gradients makes it very likely that different interpretations of the sub-grid behavior of temperature, density and velocity lead to slightly different results.

The main results of the comparison of radiative transfer codes for molecular lines can be summarized as follows.

- All relevant methods currently used in molecular astrophysics agree to a few % for optical depths up to $\tau \sim 4800$. At high optical depth and in transition layers between collision-dominated and radiation-dominated excitation, relative differences up to 2% can arise for well defined

"simple" problems. In practice, for more complex models, the relative differences are higher due to gridding and geometry problems, reaching relative differences up to 12% locally for the high optical depth model described in this paper (problem 2b). However, in most practical applications in molecular astrophysics the optical depths are lower than in our test problems, and therefore this 12% error can be regarded as an upper limit.

- The error bars on the line profiles are generally much less than 10%, and therefore lie within the calibration errors of typical (sub-)mm observations. Only in the worst case these errors may be comparable to the observational uncertainty.
- The choice of gridding is of extreme importance, and is one of the major causes of the deviations in the problems presented. Special care should be taken when constructing models for specific problems.
- Abundances and excitation temperatures derived from lines which are formed in the transition layer should be interpreted with caution.
- The direct comparison of results of different programs speeds up significantly the debugging process of new programs.

The work presented here is one step in the direction of standardization of radiative transfer computations in molecular rotational lines. Suggestions for future work in this area include: (1) establishment of a database for collisional rate coefficients, accessible to the community through the WWW; (2) a campaign to have inelastic rate coefficients measured or calculated for those molecules for which these data are unavailable, and (3) comparison of 2D radiative transfer codes, with a test problem based on, e.g., the rotating flattened collapse described by Terebey et al. (1984) or the "sheet" models of protostellar collapse by Hartmann et al. (1996). These developments will be vital to interpreting the high-quality data which

e.g. HIFI (the heterodyne instrument onboard the Herschel Space Observatory) and ALMA will provide.

References

Auer, L. H. 1987, Numerical Radiative Transfer, ed. W. Kalhofen (Cambridge University Press), 101

Bernes, C. 1979, A&A, 73, 67

Black, J. H. 2000, Astrochemistry: From Molecular Clouds to Planetary Systems, ed. Y. C. Minh, & E. F. van Dishoeck (San Francisco: ASP), IAU Symp., 197, 81

Choi, M., Evans, N. J., Gregersen, E. M., & Wang, Y. 1995, ApJ, 448, 742

Dullemond, C. P., & Turolla, R. 2000, A&A, 360, 1187

Dullemond, C. P. 1999, Ph.D. Thesis, University of Leiden

Green, S. 1975, ApJ, 201, 366

Harper, G. M. 1994, MNRAS, 268, 894

Hartmann, L., Calvet, N., & Boss, A. 1996, ApJ, 464, 387

Hartstein, D., & Liseau, R. 1998, A&A, 332, 703

Hauschildt, P. H., Störzer, H., & Baron, E. 1994, JQSRT, 51, 875

Hogerheijde, M. R., & van der Tak, F. F. S. 2000, A&A, 362, 697

Juvela, M. 1997, A&A, 322, 943

Martin, H. M., Hills, R. E., & Sanders, D. B. 1984, MNRAS, 208, 35

Mihalas, D. 1978, Stellar Atmospheres, 2nd ed. (San Francisco: Freeman)

Monteiro, T. S. 1985, MNRAS, 214, 419

Myers, P. C., Evans, N. J., & Ohashi, N. 2000, Protostars and Planets IV, 217

Ng, K. 1974, J. Chem. Phys., 61, 2680

Olson, G. L., Auer, L. H., & Buchler, J. R. 1986, J. of Quant. Spectrosc. and Rad. Transf., 35, 431

Olson, G. L., & Kunasz, P. B. 1987, J. of Quant. Spectrosc. and Rad. Transf., 38, 325

Ossenkopf, V., Trojan, C., & Stutzki, J. 2001, A&A, 378, 608

Park, Y.-.S., & Hong, S. S. 1998, ApJ, 494, 605

Rawlings, J. M. C., Taylor, S. D., & Williams, D. A. 2000, MNRAS, 313, 461

Rawlings, J. M. C., & Yates, J. A. 2001, MNRAS, 326, 1423

Rybicki, G. B., & Lightman, A. P. 1979, Radiative Processes in Astrophysics (New York: Wiley)

Rybicki, G. B., & Hummer, D. G. 1991, A&A, 245, 171

Rybicki, G. B., & Hummer, D. G. 1992, A&A, 262, 209

Scharmer, G. B., & Carlsson, M. 1985, in Progress in Stellar Spectral Line Formation Theory, NATO ASIC Proc. 152, ed. J. E. Beckman, & L. Crivellari (Dordrecht: Reidel), 189

Schöier, F. L. 2000, Ph.D. Thesis, University of Stockholm

Shu, F. H. 1977, ApJ, 214, 488

Steinacker, J., Thamm, E., & Maier, U. 1996, J. of Quant. Spectrosc. and Rad. Transf., 56, 97

Terebey, S., Shu, F. H., & Cassen, P. 1984, ApJ, 286, 529

Wiesemeyer, H. 1997, Ph.D. Thesis Max-Planck Institut für Radioastronomie and Bonn University